PAPER

Theoretical investigation on Pt(II)- and Au(I)-mediated cycloisomerizations of propargylic 3-indoleacetate: [3 + 2]- versus [2 + 2]-cycloaddition products†

Yuxia Liu,[a] Dongju Zhang,*[a] Siwei Bi[b] and Chengbu Liu[a]

With the aid of density functional theory (DFT) calculations, we have performed a detailed mechanism study for the catalytic cycloisomerization reactions of propargylic 3-indoleacetate to better understand the observed divergent reactivities of two catalysts, $PtCl_2$ and $(PPh_3)AuSbF_6$, which result in [3 + 2]- and [2 + 2]-cycloaddition products, respectively. The calculated results confirm that the lactone intermediates are common and necessary species for the formation of the two products and that $PtCl_2$ and (PH_3)-$AuSbF_6$ respectively favor the formation of the [3 + 2]- and [2 + 2]-products. The intrinsic reasons for the divergent reactivities of the two catalysts have been analyzed in detail. We believe that the essentially different metal–ligand interactions in $PtCl_2$ and $(PPh_3)AuSbF_6$ are mainly responsible for their divergent regioselectivities, while the solvent effects have little impact on the catalyst activity. Starting from lactone intermediates, $PtCl_2$ induces the intramolecular nucleophilic addition to give the [3 + 2] cycloisomerization product due to the strong π-electron-donating ability of chlorine ligands, while $(PPh_3)AuSbF_6$ results in the intramolecular nucleophilic addition reaction to form the [2 + 2] cycloisomerization product because of the strong σ-electron-donating ability of phosphine ligands.
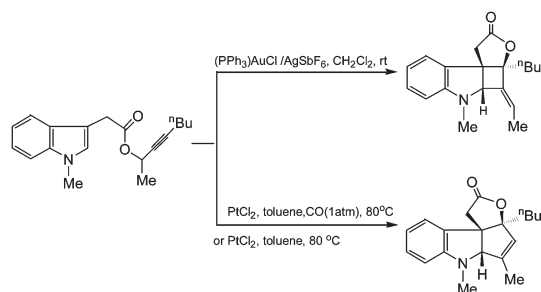
1. Introduction

Transition-metal catalyzed organic chemistry has increasingly emerged as a powerful tool for the synthesis of various carbo- and hetero-cyclic molecules in the past few decades.[1–7] Particularly, complexes derived from late transition metals Pt and Au have exhibited exceptional potential to activate C–C unsaturated bonds towards the intra- or inter-molecular nucleophilic addition of alkenes, arenes, ethers, and carbonyl groups, triggering a variety of organic transformations.[8–13] In general, Pt(II) catalysts, mostly $PtCl_2$, show similar reactivity to cationic Au(I) catalysts.[14–17] And there are few examples for catalytic divergence of these two complexes.[18]

Recently, Zhang and co-workers[19,20] successively reported the cycloisomerization reactions of propargylic 3-indoleacetate mediated by the two transition metal catalysts. As shown in

Scheme 1, in the presence of a Au(I) salt, $(PPh_3)AuSbF_6$, generated *in situ* from the mixture of $(PPh_3)AuCl$ and $AgSbF_6$, the reaction took place in dichloromethane solution at ambient temperature, affording highly functionalized 2,2-indoline-fused cyclobutane ([2 + 2]-cycloaddition product) in 83% isolated yield.[19] While $PtCl_2$ was used to catalyze the reaction, 2,3-indoline-fused cyclopentene ([3 + 2]-cycloaddition product) was unexpectedly isolated in a yield of 94% with 1 atm of CO in toluene at 80 °C.[20] Both reactions are of great importance, and provide efficient access to densely functionalized tetra-cyclic structures, a significant starting point of synthesizing indoline-containing alkaloids. Furthermore, the synthetic potential of the methodology has been partly demonstrated by
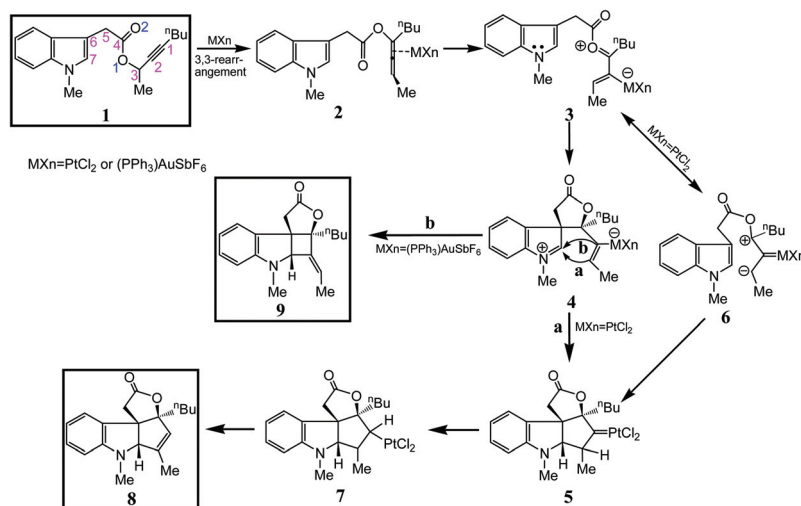
[a] *Key Lab of Colloid and Interface Chemistry, Ministry of Education, Institute of Theoretical Chemistry, Shandong University, Jinan, 250100, P.R. China.*
E-mail: zhangdj@sdu.edu.cn; Fax: (+86) 531-88564464
[b] *College of Chemistry and Chemical Engineering, Qufu Normal University, Qufu 273165, P.R. China*

†Electronic supplementary information (ESI) available: Optimized geometries with selected structural parameters and Cartesian coordinates for all the species involved in the reaction, as well as comparison of the structural parameters in gas phase of the several key species calculated using B3LYP and B97D functionals. See DOI: 10.1039/c2ob26691a

Scheme 1 The $PtCl_2$- and $(PPh_3)AuSbF_6$-catalyzed cycloisomerization reactions of propargylic 3-indoleacetate reported by Zhang and co-workers.[19,20]

Scheme 2 The proposed pathways by Zhang and co-workers for the formation of [3 + 2]-cycloaddition product **8** and [2 + 2]-cycloaddition product **9** from the cycloisomerizations of propargylic 3-indoleacetate **1** catalyzed by PtCl$_2$ and (PPh$_3$)AuSbF$_6$, respectively.

synthesizing the tetracyclic core of vindolinine.[20] To account for the observed different products, Zhang et al. postulated possible reaction mechanisms, as summarized in Scheme 2, where both the (PPh$_3$)AuSbF$_6$- and PtCl$_2$-catalyzed reactions start from the 3,3-rearrangement (i.e., the O2 atom binds to the C1 atom with the simultaneous cleavage of the O1–C3 bond) of the propargylic ester in **1**, giving complex **2**, which evolves into the metal-containing lactone intermediate **4**. And then, the C2 atom or the C3 atom in **4** nucleophilically attacks the C7 atom, resulting in [2 + 2]-cycloaddition product **9** or [3 + 2]-cycloaddition product **8**.

Despite the importance of the catalytic cycloisomerizations, the actual reason why (PPh$_3$)AuSbF$_6$ and PtCl$_2$ result in the different products has not been well understood yet, and the fundamental mechanisms involved in the cycloisomerizations induced by the two catalysts also remain unclear. It is known that the mechanism details of a reaction are not easily accessible by experiment. Alternatively, theoretical calculations based on first principles can aid our understanding of the reaction mechanism at the atomic and molecular levels. Herein, we present a density functional theory (DFT) study on the cycloisomerization reactions of propargylic 3-indoleacetate catalyzed by both (PPh$_3$)AuSbF$_6$ and PtCl$_2$, from which we expected to understand the different catalytic reactivities of the two catalysts.

2. Computational details

All the calculations presented were carried out in the framework of density functional theory (DFT) employing the B3LYP functional.[21–24] Accurate theoretical calculations based on DFT have been used extensively to study various chemical reactions.[25,26] In the present calculations, the standard 6-31G (d, p) basis set was used for C, H, N, O, F, P and Cl atoms, whereas the effective core potentials (ECP) of Hay and Wadt

combined with double-ζ valence basis sets (LanL2DZ)[27–29] were used to describe Au, Sb and Pt atoms. Full geometry optimizations of minima and transition states were performed at the selected level of theory, and the transition states located were checked by performing the intrinsic reaction coordinate (IRC)[30,31] calculations to confirm that each of them actually connects the desired reactant and product. Harmonic vibrational frequency calculations at the same level of theory have also been conducted to verify all stationary points as minima (zero imaginary frequencies) or first-order saddle points (one imaginary frequency) and to provide free energies at 298.15 K, which include entropic contributions by taking into account the vibrations, rotations, and translations of the structures.
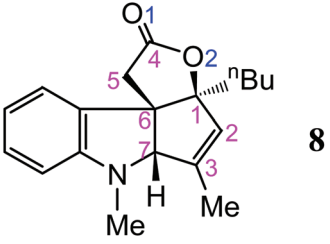
Solvent effects have also been taken into account at the same DFT level by calculating the single-point energies of the geometries obtained in the gas-phase by employing the simple self-consistent reaction field (SCRF) method[32–34] based on the polarizable continuum model (PCM)[35,36] with UAKS cavities.[37] Here, the solvent used is toluene for the Pt(II)-catalyzed system and dichloromethane for the Au(I) system, corresponding to the respective experimental conditions. All the calculations in this paper were implemented with the Gaussian-03 software package.[38] Calculations for several selected structures shown in Table S1† are also performed using the dispersion-corrected B97D functional[39] with the Gaussian-09 software package.[40]

3. Results and discussion

To calibrate the quality of the calculations in the present work, we compare the calculated geometrical parameters of product **8** with the corresponding experimental values given by Zhang et al.[20] As shown in Table 1, the maximum relative error between theoretical values and experimental data is only 0.9%. Furthermore, we performed additional calculations using the

dispersion-corrected B97D functional for several structures, including 4^{Pt}, $TS9^{Pt}$, and $TS11^{Pt}$ in Scheme 4, and 4^{Au}, $TS9^{Au}$, and $TS11^{Au}$ in Fig. 2. The optimized geometries are schematically shown in Table S1,† where the crucial parameters are compared with those from the B3LYP calculations. It is obvious that the B3LYP functional gives almost the same geometries as the B97D functional. These facts along with the previous finding that the B3LYP functional can successfully describe Au- and Pt-catalyzed organometallic systems[41–44]

Table 1 Calculated and experimental geometrical parameters (in Å) of [3 + 2]-cycloaddition product **8**

| Bond	r_{calc}[a]	r_{expt}[b].	Δr[c]	Δr[d]
C1–C2	1.508	1.504	0.004	0.3%
C2–C3	1.337	1.336	0.001	0.1%
C3–C7	1.520	1.514	0.006	0.4%
C6–C7	1.562	1.550	0.012	0.8%
N–C7	1.481	1.475	0.006	0.4%
C5–C6	1.538	1.530	0.008	0.5%
C4–C5	1.521	1.507	0.014	0.9%
O1–C4	1.204	1.203	0.001	0.1%
O2–C4	1.357	1.352	0.005	0.4%
C1–O2	1.458	1.468	0.010	0.7%

[a] Calculated values. [b] Experimental values. [c] Absolute errors. [d] Relative errors.

make us confident about the reliability and accuracy of the level of theory used in the present work.

In the following sections, we show calculated results for the cycloisomerization reactions of propargylic 3-indoleacetate catalyzed by $PtCl_2$ and $(PPh_3)AuSbF_6$, respectively. Our discussion will exclusively focus on the solvent results unless otherwise stated. For each catalytic system, we have calculated two pathways resulting in products **8** and **9** (Scheme 2). According to the proposal of Zhang and co-workers[20] shown in Scheme 2, the common and necessary intermediate forming product **8** and product **9** is structure **4**, from which the reaction evolves into **8** in the presence of $PtCl_2$ or **9** in the presence of (PPh_3)-$AuSbF_6$. Thus our discussion on each system is divided into two subsections: from **1** to **4** and from **4** to **8** or **9**. For clarity, structures shown in Scheme 2 (**1–9**), and intermediates (**IM**s) and transition states (**TS**s) located in the present calculations are marked with superscripts "Pt" and "Au", implying the $PtCl_2$- and $(PPh_3)AuSbF_6$-involving structures, respectively.

We first examined the $PtCl_2$-mediated isomerization reaction, in which it was found that the reaction favors the formation of the [3 + 2]-cycloaddition product **8** in both the presence and absence of CO. It should be expected that CO would form the stable transition metal complex $PtCl_2(CO)_n$ with $PtCl_2$ due to its strong interaction with the Pt(II) center. However, in the present reaction, the CO ligands in $PtCl_2(CO)_n$ only play a role of spectator. This situation is similar to the mechanism proposed by Fürstner *et al.* in a $PtCl_2$-catalyzed rearrangement of methylenecyclopropanes.[45] In addition, the experimental results of Zhang *et al.*[20] indicated that the reaction also proceeded smoothly even without the presence of CO. Based on these considerations, our present calculations omitted the effect of CO on the reactivity.

In Scheme 3, we collected the calculated results leading to 4^{Pt}. The optimized geometries with selected structural
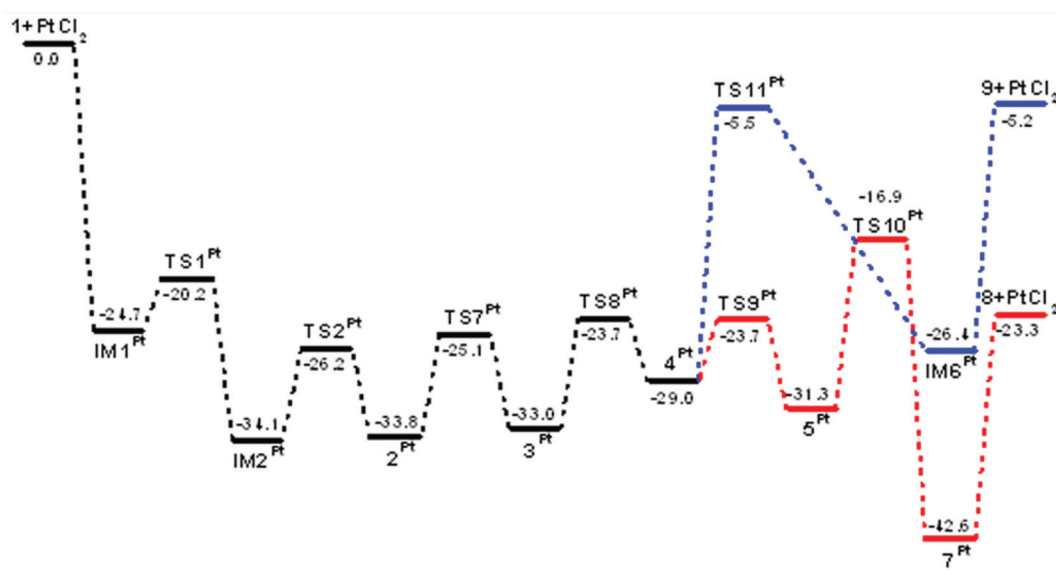
Fig. 1 Calculated free energy profiles in toluene solvent for forming both [3 + 2]-(red line) and [2 + 2]-(blue line) cycloaddition products from the $PtCl_2$-catalyzed reaction of propargylic 3-indoleacetate. The relative free energies are given in kcal mol^{-1}.
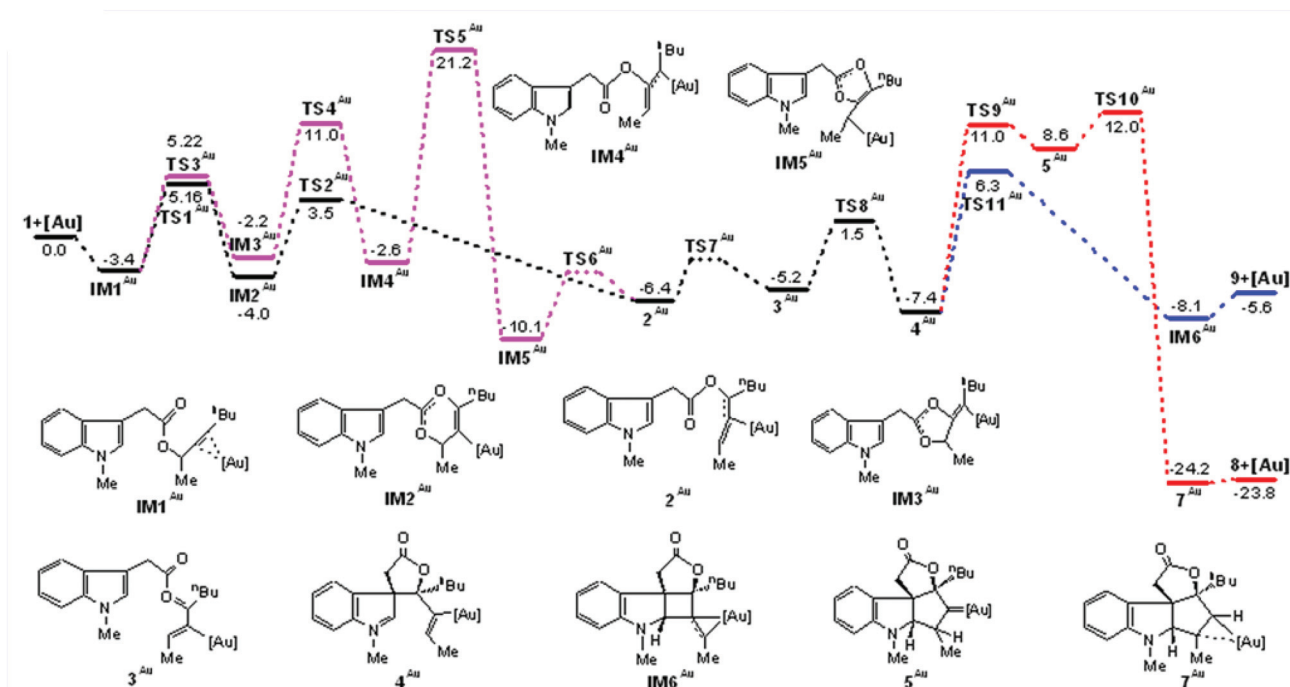
Fig. 2 Calculated free energy profiles in CH_2Cl_2 solvent for forming both [3 + 2]-(red line) and [2 + 2]-(blue line) cycloaddition products from the $(PH_3)AuSbF_6$-catalyzed reaction. The relative free energies are given in kcal mol^{-1}.
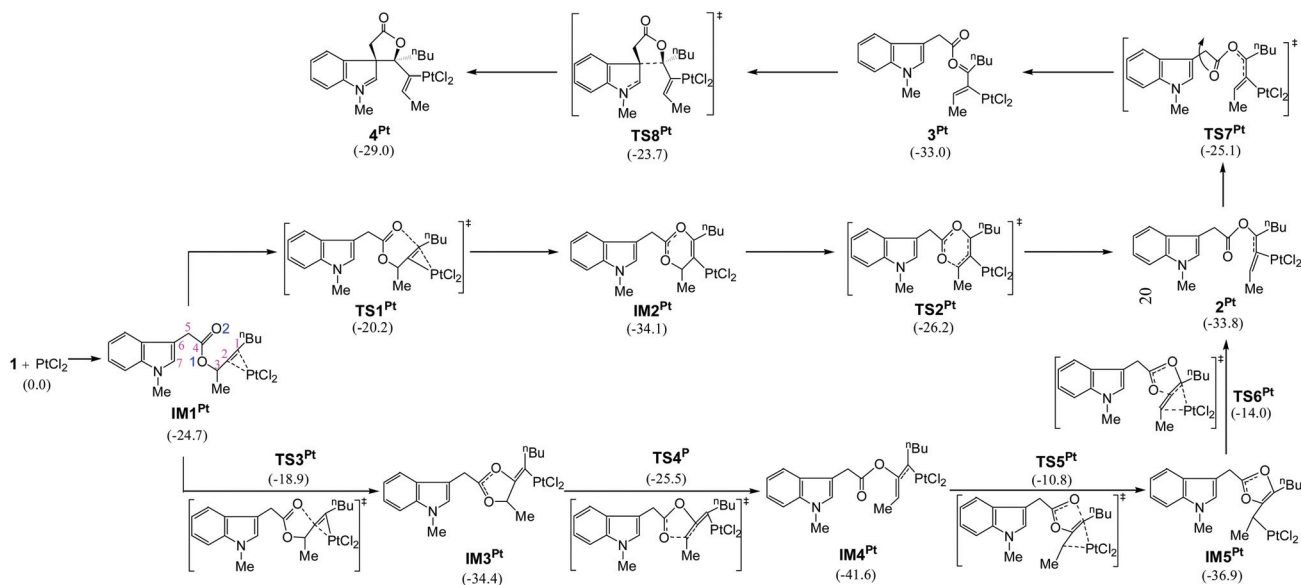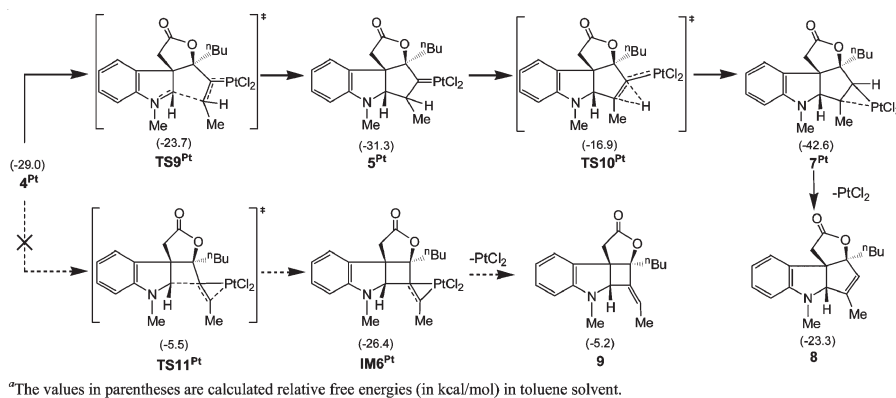

^{a}The values in parentheses are calculated relative free energies (in kcal/mol) in toluene solvent.

Scheme 3 The schematic geometries for species involved in the formation of Pt-containing lactone 4^{Pt}. The values in parentheses are calculated relative free energies (in kcal/mol) in toluene solvent.

parameters for the species involved in Scheme 3 are illustrated in Fig. S1.† As is seen in Scheme 3, at the entrance of the reaction, the coordination of catalyst $PtCl_2$ to the C≡C bond of substrate **1** affords Pt(II)–alkyne complex $IM1^{Pt}$, inducing the triple bond towards the nucleophilic attack by the carbonyl O2 atom. The coordination process is calculated to be exergonic

by 24.7 kcal mol^{-1}. The transformation of $IM1^{Pt}$ to carboxyalelne 2^{Pt}, as proposed in Scheme 2, involves two elementary steps. The first step involves the nucleophilic addition of the carbonyl O2 atom to the external C1 atom of the alkynyl moiety in $IM1^{Pt}$ via a six-membered cyclization transition state $TS1^{Pt}$ to yield energetically more stable intermediate $IM2^{Pt}$

This journal is © The Royal Society of Chemistry 2013

Org. Biomol. Chem., 2013, **11**, 336–343 | **339**

Scheme 4 The schematic geometries for species involved along the two branches from **4^Pt** to form [3 + 2]-cycloaddition product **8** and [2 + 2]-cycloaddition product **9**. The values in parentheses are calculated relative free energies (in kcal/mol) in toluene solvent.

with a barrier of 4.5 kcal mol^{-1}. In the case of the second step, through a six-membered ring-opened transition state **TS2^Pt**, the O1–C3 bond of **IM2^Pt** cleaves, leading to the 3,3-rearrangement product **2^Pt**. The barrier involved in this ring-opening step is calculated to be 7.9 kcal mol^{-1}. Note that the Pt–C2 and C1–C2 bond lengths in **2^Pt** shown in Fig. S1† are calculated to be 1.988 and 1.436 Å, respectively, which are much longer than the corresponding ones in **IM2^Pt** (1.944 and 1.334 Å), implying that the C1 atom is remarkably activated upon σ-coordination of the PtCl$_2$ catalyst to the center C2 atom of the allene moiety. In addition, as proposed in a previous study,[46] the O2 atom in **IM1^Pt** can also nucleophilically attack the alkynyl internal C2 atom *via* a five-membered transition state **TS3^Pt**, providing intermediate **IM3^Pt**. The energy demand from **IM1^Pt** to **TS3^Pt** is calculated to be 5.8 kcal mol^{-1}. In the next step, the cleavage of the O1–C3 bond in **IM3^Pt** takes place with an energy requirement of 8.9 kcal mol^{-1}, through the five-membered ring-opened transition state **TS4^Pt**, resulting in **IM4^Pt**. And subsequently, the O1 atom in **IM4^Pt** nucleophilically attacks the C1 atom *via* **TS5^Pt** with a barrier of 30.8 kcal mol^{-1}, affording intermediate **IM5^Pt**, from which complex **2^Pt** is achieved by breaking the O2–C2 bond *via* **TS6^Pt** with a barrier of 22.9 kcal mol^{-1}. The highest barrier required along the alternative five-membered cyclization route is 30.8 kcal mol^{-1} (corresponding to the conversion from **IM4^Pt** to **IM5^Pt**), which is substantially higher than the barrier of 7.9 kcal mol^{-1} involved in the conversion from **IM2^Pt** to **2^Pt**. Therefore, it is clear that the six-membered cyclization route is energetically much more favorable than the five-membered cyclization one. (A similar situation is also found for the Au-catalyzed system, as seen in Fig. 2, where the energy barrier for the process **IM4^Au** →**IM5^Au** is 23.8 kcal mol^{-1}, which is significantly higher than the barrier of 8.6 kcal mol^{-1} involved in the transformation from **IM1^Au** to **IM2^Au**.)

In order to facilitate the subsequent interaction of C1 with C6, **2^Pt** has to evolve into slightly unstable isomer **3^Pt** by rotating the carbonyl group along the C4–O2 single bond. The σ-rotation step *via* **TS7^Pt** requires overcoming an energy barrier of 8.7 kcal mol^{-1}. In **3^Pt**, the interaction between the lone pair

p orbital of the N atom and the empty π* orbital of the C6–C7 double bond significantly increases the electron density on the C6 atom. The calculated natural bond orbital (NBO) charge on C6 in **3^Pt** is −0.149 e, facilitating the electrophilic attack of the C1 atom carrying positive charge (0.601 e). **TS8^Pt** is the transition state structure concerning the C1–C6 bond formation, and its forward product is the five-membered cyclization lactone **4^Pt**, which lies below the reaction entrance by 29.0 kcal mol^{-1}. The barrier from **3^Pt** to **TS8^Pt** is calculated to be 9.3 kcal mol^{-1}. The calculated energy profile forming **4^Pt** is given in black line in Fig. 1.

Note that we also tried to search for a direct transformation from **2^Pt** to **4^Pt** without involving **3^Pt**. The calculated results show that with decreasing indole–allene proximal carbon distance (C1–C6 distance), the carbonyl group in **2^Pt** rotates along the C4–O2 single bond. As a result, **2^Pt** proceeds to **3^Pt**. This fact indicates that **3^Pt** is a necessary intermediate for the transformation from **2^Pt**. Thus the direct transformation pathway from **2^Pt** to **4^Pt** without involving **3^Pt** cannot be located in the present work.

Starting from **4^Pt**, we calculated two reaction branches forming [3 + 2]-cycloaddition product **8** and [2 + 2]-cycloaddition product **9**, respectively. Scheme 4 presents the schematic structures involved and calculated relative energies. And the corresponding optimized geometries with selected structural parameters are illustrated in Fig. S2.† Concerning the formation of **8**, Zhang *et al.* presumed (Scheme 2) that lactone **4^Pt** converts to Pt-carbenoid **5^Pt** by performing the nucleophilic addition of the C3 atom to the C7 atom, finally to product **8** *via* a direct 1,2-H shift in **5^Pt**. Our theoretical results indicate that starting from **4^Pt**, the C3 atom nucleophilically attacks the C7 atom *via* a five-membered ring transition state, **TS9^Pt**, with a barrier of only 5.3 kcal mol^{-1}, yielding **5^Pt** with a character of Pt-carbenoid. In this process, the binding of C3 with the C7 atom weakens its π-interaction with the C2 atom, which, conversely, promotes the pπ–dπ orbital overlap between the C2 atom and the Pt center, thereby leading to the Pt=C2 carbenoid character. As indicated in Fig. S2,† the length of the C2–Pt bond in **5^Pt** is 1.833 Å, considerably shorter than that of the

corresponding single bond in 4^{Pt} (1.977 Å). In Scheme 2, Zhang et al.[20] proposed that carbenoid 5^{Pt} can be also obtained via an imagined 1,3-dipolar intermediate (6), a resonance structure of oxocarbenium 3. However, the present calculations failed to locate such a structure, which always collapsed into complex 3^{Pt} upon optimization. Therefore, it is believed that the process $3^{Pt} \rightarrow 4^{Pt} \rightarrow 5^{Pt}$ is the available route leading to 5. The subsequent step is a direct 1,2-H shift, where the hydrogen initially attached to the C3 atom now migrates to the C2 atom, through transition state $TS10^{Pt}$ with a barrier of 14.4 kcal mol^{-1}, leading to catalyst–cyclopentene adduct 7^{Pt}, which lies 42.6 kcal mol^{-1} below the reaction entrance. Finally, 7^{Pt} decomposes into product 8 and the catalyst PtCl$_2$ which is recycled for the next reaction procedure. The calculated energy profile from 4^{Pt} to 8 is given in red line in Fig. 1.

Alternatively, if 4^{Pt} evolves into cyclobutane 9, the transition state and intermediate located are $TS11^{Pt}$ and $IM6^{Pt}$, whose schematic geometries are collected in Scheme 4. Along this branch, 4^{Pt} can directly transform into catalyst–cyclobutane adduct, $IM6^{Pt}$, by the nucleophilic addition of C2 to C7 via the four-membered cyclized transition state $TS11^{Pt}$. The present calculations show that the cyclization process requires overcoming a barrier of 23.5 kcal mol^{-1}. And then the PtCl$_2$ catalyst is expelled from $IM6^{Pt}$ leading to [2 + 2]-cycloaddition product 9, completing the whole catalytic cycle. The calculated relative energy profile is given in blue line in Fig. 1, from which we can clearly see that from 4^{Pt}, the energy requirement leading to [2 + 2]-cycloaddition product 9 is significantly higher than that resulting in [3 + 2]-cycloaddition product 8. Furthermore, the highest barrier for forming [3 + 2]-cycloaddition product 8 is 14.4 kcal mol^{-1}, which corresponds to the 1,2-H shift process from 5^{Pt} to 7^{Pt}. In contrast, the energy requirement corresponding to the transformation from 4^{Pt} to $IM6^{Pt}$ is 23.5 kcal mol^{-1}. In addition, the precursor of 8, 7^{Pt}, is much more stable than that of 9, $IM6^{Pt}$. These facts clearly suggest that the PtCl$_2$-catalyzed reaction preferentially proceeds along the branch leading to [3 + 2]-cycloaddition product 8. This is in agreement with the experimental observation concerning the predominant product of cyclopentene 8.

Similarly, we have also performed calculations for the (PPh$_3$)AuSbF$_6$-catalyzed reaction. It should be noted that in the experiments of Zhang et al.[20] (PPh$_3$)AuCl and AgSbF$_6$ were used as the precursors of catalyst (PPh$_3$)AuSbF$_6$ in which the anion SbF$_6^-$ plays a role of counterion to offset the cationic charge on the metal center. The silver cation (Ag$^+$) in the precursor AgSbF$_6$ neutralizes the chloride anion (Cl$^-$) in the precursor (PPh$_3$)AuCl to form the insoluble salt AgCl, which does not affect the reactivity of the catalyzed reaction. In line with previous theoretical studies,[42,47–49] the catalyst is modeled using the simplified complex (PH$_3$)AuSbF$_6$ to save the computational cost.

Fig. 2 shows the calculated potential energy profiles for forming [2 + 2]- and [3 + 2]-cycloaddition products, respectively, and Fig. S3 and S4† present the optimized geometries with selected structural parameters for the species involved in the reaction. Note that the specific locations of the SbF$_6^-$ counterion in Fig. S3 and S4† are based on the results of geometrical optimization calculations. Our present calculations have considered the different locations of SbF$_6^-$ in the proximity of the gold. The geometries shown in Fig. S3 and S4† correspond to the energetically most favorable ones.

We find that the (PH$_3$)AuSbF$_6$-catalyzed reaction involves a similar mechanism to the PtCl$_2$-catalyzed reaction. So the relevant mechanism details are not discussed again for simplification. We pay attention mainly to the relative energy profiles of the two catalytic reactions. It is noted that the large potential energy profile differences for [2 + 2]- and [3 + 2]-cycloaddition product pathways after 4^{Au} is substantially different from those in the PtCl$_2$-mediated system. As shown in Fig. 2, from 4^{Au}, the barrier forming [2 + 2]-cycloaddition product 9 is 13.7 kcal mol^{-1} (the energy difference between 4^{Au} and $TS11^{Au}$ corresponding to C2 nucleophilic addition to the C7 atom), which is lower than the overall barrier leading to [3 + 2]-cycloaddition product 8 (19.4 kcal mol^{-1}, corresponding to the energy difference between 4^{Au} and $TS10^{Au}$). This indicates that the pathway resulting in product 9 is kinetically more favorable than that resulting in product 8. However, on the other hand, product 8 is thermodynamically much more favorable than product 9, as shown in Fig. 2. Thus it seems that we should also expect product 8 rather than product 9 for the Au-catalytic process, like the PtCl$_2$-catalyzed reaction, although the barrier to form product 8 is relatively higher by 6.7 kcal mol^{-1} than that to form product 9. However, it should be noted that the Au-catalyzed reaction was carried out at room temperature in the experiments of Zhang et al.,[20] unlike the Pt-catalyzed process carried out at 80 °C. Under such a specific and appropriate temperature, the reaction may prefer to yield product 9. From the present calculated results we conjecture that the 3 + 2 product 8 may be the final product if the reaction was carried out at elevated temperatures. We believe that for the (PPh$_3$)AuSbF$_6$-catalyzed reaction, controlling the temperature is of crucial importance for obtaining the desired 2 + 2 product 9.

The different regioselectivities of PtCl$_2$ and (PPh$_3$)AuSbF$_6$ can be understood by comparatively analyzing electronic interactions in 4^{Au} and 4^{Pt}. For 4^{Au}, there exists a three-centre-four-electron bonding network[50,51] on P–Au–C2, simply denoted as [P: Au–C2 ↔ P–Au: C2]. The presence of the strong σ-electron-donating phosphine ligand (strong trans influence) significantly reduces the interaction of Au with the C2 atom, which results in an increase of the electron density on the C2 atom and hence facilitates the nucleophilic attack of the C2 atom on the electron-deficient C7 atom, resulting in the [2 + 2]-cycloaddition product 9. In contrast, the strong π-electron-donating chlorine ligands in lactone 4^{Pt} strengthen the back-donating potential of Pt and thus induce the π-electron density on the metal moving towards the C2=C3 bond. Consequently, the C3 atom is more negatively charged and inclines to perform the nucleophilic addition, giving the [3 + 2]-cycloaddition product 8. The calculated natural bond orbital (NBO) charges on structures 4^{Au} and 4^{Pt} provide further support for their different reactivities. As shown in Table 2, in 4^{Au} the charges on C2, C3

This journal is © The Royal Society of Chemistry 2013

Org. Biomol. Chem., 2013, **11**, 336–343 | **341**

Table 2 Calculated partial natural bond orbital (NBO) charges on two structures 4^{Au} and 4^{Pt}

	C1	C2	C3	C6	C7	N	Au	P	Pt
4^{Au}	0.31	−0.45	−0.23	−0.14	0.27	−0.29	0.31	0.07	/
4^{Pt}	0.30	−0.15	−0.28	−0.15	0.26	−0.29	/	/	0.51

Table 3 Calculated relative free energies (in kcal mol^{-1}) in the gas phase and in solvent for selected steps involved in the two cycloisomerization reactions catalyzed by PtCl$_2$ and (PH$_3$)AuSbF$_6$

	PtCl$_2$-catalyzed reaction		(PH$_3$)AuSbF$_6$-catalyzed reaction	
	Gas phase	In toluene	Gas phase	In CH$_2$Cl$_2$
IM1 →TS1	5.5	4.5	7.8	8.6
IM2 →TS2	7.3	7.9	7.7	7.5
2 →3	2.2	0.8	1.1	1.2
3 →TS8	12.1	9.3	8.3	6.7
4 →TS9	3.8	5.3	17.6	18.4
5 →TS10	16.2	14.4	5.0	3.4
4 →TS11	20.9	20.7	13.0	13.7

and C7 atoms are −0.43, −0.23, 0.27 e, whereas the corresponding ones in 4^{Pt} are −0.15, −0.28, 0.26 e. So (PH$_3$)AuSbF$_6$ leads to the C2 attack product (**9**), while PtCl$_2$ favors C3 addition product (**8**), which is closely related to the different electron-donating ways of the ligands on two catalysts.

Secondly, we find that Au-carbenoid 5^{Au} is much less stable than 4^{Au} (8.6 *vs.* −7.4 kcal mol^{-1}), which is again very different from the PtCl$_2$-catalyzed system, where 5^{Pt} presents higher stability than 4^{Pt} (−31.3 *vs.* −29.0 kcal mol^{-1}). This also originates from the different electron-donating ways of the ligands on these two catalysts. The resulting weak interaction of Au with C2 in 5^{Au} does not favor generation of Au=C2 carbenoid, while the π back-donation of Pt in 5^{Pt} significantly contributes to the formation of Pt carbenoid, facilitating the formation of **8**. In addition, the forward evolution of energy-rich intermediates 5^{Au} to 7^{Au} has a slightly higher barrier relative to its reverse transformation to intermediate 4^{Au} (3.4 *vs.* 2.4 kcal mol^{-1}). Therefore, 5^{Au}, if formed, would reversibly return to complex 4^{Au} rather than evolve into 7^{Au}, in agreement with the formation of product **9** as (PPh$_3$)AuSbF$_6$ is used as the catalyst.

Thirdly, it is clear that the calculated energy profile of the (PH$_3$)AuSbF$_6$-catalyzed reaction is much higher than that of the PtCl$_2$-catalyzed system. For the latter, all intermediates and transition states lie below the reaction entrance. While for the former, almost all of the transition states lie above the reaction entrance. This may be due to the steric hindrance resulting from the large bulk of the counterion SbF$_6^-$ on the Au catalyst.

Finally, to evaluate the influence of the solvent effect on the reactivities, we have calculated the relative energies of several selected steps involved in the two cycloisomerization reactions catalyzed by PtCl$_2$ and (PH$_3$)AuSbF$_6$. As shown in Table 3, the calculated relative energy differences between the PCM and gas phase calculations are small, implying that the solvent effect has little influence on the reactivity.

4. Conclusions

The detailed elementary step mechanisms of PtCl$_2$- and (PH$_3$)AuSbF$_6$-catalyzed cycloisomerization reactions of propargylic 3-indoleacetates have been studied by performing DFT calculations to rationalize the observed divergent reactivities of two catalysts. The reaction is initiated by the Pt(II) or Au(I) coordination to the alkynyl moiety of the substrate, resulting in a 3,3-rearrangement intermediate, which further converts to the Pt- or Au-containing lactone through cyclization of the oxonium group to the indole 3-position. After that, the reaction proceeds either *via* five-membered cyclization with a subsequent 1,2-H shift to form a [3 + 2]-cycloaddition product or *via* four-membered cyclization to form a [2 + 2]-cycloaddition product depending on the catalysts used. PtCl$_2$ favors the formation of the [3 + 2] product, while (PH$_3$)AuSbF$_6$ prefers to give the [2 + 2] product. The divergent regioselectivities of two catalysts intrinsically originate from their different metal–ligand interactions. In PtCl$_2$, the strong π-electron-donating chlorine ligands induce the intramolecular nucleophilic addition to give the [3 + 2] cycloisomerization product, while in (PPh$_3$) AuSbF$_6$, the strong σ-electron-donating phosphine ligand results in the intramolecular nucleophilic addition reaction to form the [2 + 2] cycloisomerization product. The solvent effects have little impact on the catalyst reactivities.

Acknowledgements

References

1 J. C. Lewis, R. G. Bergman and J. A. Ellman, *Acc. Chem. Res.*, 2008, **41**, 1013–1025.

2 S. F. Kirsch, *Synthesis*, 2008, **2008**, 3183–3204.

3 M. Meldal and C. W. Tornøe, *Chem. Rev.*, 2008, **108**, 2952–3015.

4 V. Michelet, P. Y. Toullec and J. P. Genêt, *Angew. Chem., Int. Ed.*, 2008, **47**, 4268–4315.

5 N. Patil and Y. Yamamoto, *Chem.–Eur. J.*, 2008, **14**, 5382–5391.

6 K. C. Majumdar, P. Debnath and B. Roy, *Heterocycles*, 2009, **78**, 2661–2728.

7 S. M. A. Sohel and R. S. Liu, *Chem. Soc. Rev.*, 2009, **38**, 2269–2281.

8 B. Crone and S. F. Kirsch, *Chem.–Eur. J.*, 2008, **14**, 3514–3522.

9 A. Arcadi, *Chem. Rev.*, 2008, **108**, 3266.

342 | *Org. Biomol. Chem.*, 2013, **11**, 336–343

This journal is © The Royal Society of Chemistry 2013

10 Z. Li, C. Brouwer and C. He, *Chem. Rev.*, 2008, **108**, 3239.

11 D. J. Gorin, B. D. Sherry and F. D. Toste, *Chem. Rev.*, 2008, **108**, 3351.

12 A. Fürstner, *Chem. Soc. Rev.*, 2009, **38**, 3208–3221.

13 A. S. K. Hashmi, *Angew. Chem., Int. Ed.*, 2010, **49**, 5232–5241.

14 V. Mamane, T. Gress, H. Krause and A. Fürstner, *J. Am. Chem. Soc.*, 2004, **126**, 8654–8655.

15 B. A. B. Prasad, F. K. Yoshimoto and R. Sarpong, *J. Am. Chem. Soc.*, 2005, **127**, 12468–12469.

16 B. P. Taduri, S. M. A. Sohel, H. M. Cheng, G. Y. Lin and R. S. Liu, *Chem. Commun.*, 2007, 2530–2532.

17 K. Cariou, B. Ronan, S. Mignani, L. Fensterbank and M. Malacria, *Angew. Chem.*, 2007, **119**, 1913–1916.

18 A. S. K. Hashmi, E. Kurpejovic, W. Frey and J. W. Bats, *Tetrahedron*, 2007, **63**, 5879–5885.

19 L. Zhang, *J. Am. Chem. Soc.*, 2005, **127**, 16804–16805.

20 G. Zhang, V. J. Catalano and L. Zhang, *J. Am. Chem. Soc.*, 2007, **129**, 11358–11359.

21 M. Frisch, G. Trucks, H. Schlegel, G. Scuseria, M. Robb, J. Cheeseman, J. Montgomery Jr., T. Vreven, K. Kudin and J. Burant, *J. Chem. Phys.*, 1993, **98**, 5648–5652.

22 B. Miehlich, A. Savin, H. Stoll and H. Preuss, *Chem. Phys. Lett.*, 1989, **157**, 200–206.

23 C. Lee, W. Yang and G. Parr, *Phys. Rev.*, 1988, 785–794.

24 P. J. Stephens, F. J. Devlin and C. F. Chabalowski, *J. Phys. Chem.*, 1994, **98**, 11623–11627.

25 W. Yu, J. Hu, F. Xu, X. Sun, R. Gao, Q. Zhang and W. Wang, *Environ. Sci. Technol.*, 2011, **45**, 1917–1925.

26 F. Xu, W. Yu, Q. Zhou, R. Gao, X. Sun, Q. Zhang and W. Wang, *Environ. Sci. Technol.*, 2011, **45**, 643–650.

27 P. J. Hay and W. R. Wadt, *J. Chem. Phys.*, 1985, **82**, 270–283.

28 P. J. Hay and W. R. Wadt, *J. Chem. Phys.*, 1985, **82**, 299–310.

29 W. R. Wadt and P. J. Hay, *J. Chem. Phys.*, 1985, **82**, 284–298.

30 K. Fukui, *J. Phys. Chem.*, 1970, **74**, 4161–4163.

31 K. Fukui, *Acc. Chem. Rev.*, 1981, **14**, 363–368.

32 O. Tapia, *J. Math. Chem.*, 1992, **10**, 139–181.

33 J. Tomasi and M. Persico, *Chem. Rev.*, 1994, **94**, 2027–2094.

34 B. Y. Simkin and I. Sheikhet, *Quantum Chemical and Statistical Theory of Solutions – A Computational Approach*, Ellis Horwood, London, 1995.

35 M. Cossi, V. Barone, R. Cammi and J. Tomasi, *Chem. Phys. Lett.*, 1996, **255**, 327–335.

36 V. Barone, M. Cossi and J. Tomasi, *J. Comput. Chem.*, 1998, **19**, 404–407.

37 Y. Takano and K. N. Houk, *J. Chem. Theory Comput.*, 2005, **1**, 70–77.

38 M. J. Frisch, G. W. Trucks, H. B. Schlegel, G. E. Scuseria, M. A. Robb, J. R. Cheeseman, J. A. Montgomery, Jr., T. Vreven, K. N. Kudin, J. C. Burant, J. M. Millam, S. S. Iyengar, J. Tomasi, V. Barone, B. Mennucci, M. Cossi, G. Scalmani, N. Rega, G. A. Petersson, H. Nakatsuji, M. Hada, M. Ehara, K. Toyota, R. Fukuda, J. Hasegawa, M. Ishida, T. Nakajima, Y. Honda, O. Kitao, H. Nakai, M. Klene, X. Li, J. E. Knox, H. P. Hratchian, J. B. Cross, V. Bakken, C. Adamo, J. Jaramillo, R. Gomperts, R. E. Stratmann, O. Yazyev, A. J. Austin, R. Cammi, C. Pomelli, J. W. Ochterski, P. Y. Ayala, K. Morokuma, G. A. Voth, P. Salvador, J. J. Dannenberg, V. G. Zakrzewski, S. Dapprich, A. D. Daniels, M. C. Strain, O. Farkas, D. K. Malick, A. D. Rabuck, K. Raghavachari, J. B. Foresman, J. V. Ortiz, Q. Cui, A. G. Baboul, S. Clifford, J. Cioslowski, B. B. Stefanov, G. Liu, A. Liashenko, P. Piskorz, I. Komaromi, R. L. Martin, D. J. Fox, T. Keith, M. A. Al-Laham, C. Y. Peng, A. Nanayakkara, M. Challacombe, P. M. W. Gill, B. Johnson, W. Chen, M. W. Wong, C. Gonzalez and J. A. Pople, Gaussian, Inc., Wallingford, CT, 2004.

39 S. Grimme, *J. Comput. Chem.*, 2006, **27**, 1787–1799.

40 M. J. Frisch, G. W. Trucks, H. B. Schlegel, G. E. Scuseria, M. A. Robb, J. R. Cheeseman, G. Scalmani, V. Barone, B. Mennucci, G. A. Petersson, H. Nakatsuji, M. Caricato, X. Li, H. P. Hratchian, A. F. Izmaylov, J. Bloino, G. Zheng, J. L. Sonnenberg, M. Hada, M. Ehara, K. Toyota, R. Fukuda, J. Hasegawa, M. Ishida, T. Nakajima, Y. Honda, O. Kitao, H. Nakai, T. Vreven, J. A. Montgomery, Jr., J. E. Peralta, F. Ogliaro, M. Bearpark, J. J. Heyd, E. Brothers, K. N. Kudin, V. N. Staroverov, T. Keith, R. Kobayashi, J. Normand, K. Raghavachari, A. Rendell, J. C. Burant, S. S. Iyengar, J. Tomasi, M. Cossi, N. Rega, J. M. Millam, M. Klene, J. E. Knox, J. B. Cross, V. Bakken, C. Adamo, J. Jaramillo, R. Gomperts, R. E. Stratmann, O. Yazyev, A. J. Austin, R. Cammi, C. Pomelli, J. W. Ochterski, R. L. Martin, K. Morokuma, V. G. Zakrzewski, G. A. Voth, P. Salvador, J. J. Dannenberg, S. Dapprich, A. D. Daniels, O. Farkas, J. B. Foresman, J. V. Ortiz, J. Cioslowski and D. J. Fox, *GAUSSIAN 09 (Revision B.01)*, Gaussian Inc., Wallingford, CT, 2010.

41 Y. Xia and G. Huang, *J. Org. Chem.*, 2010, **75**, 7842–7854.

42 A. González Pérez, C. Silva López, J. Marco-Contelles, O. Nieto Faza, E. Soriano and A. R. de Lera, *J. Org. Chem.*, 2009, **74**, 2982–2991.

43 Y. T. Lee, Y. K. Kang and Y. K. Chung, *J. Org. Chem.*, 2009, **74**, 7922–7934.

44 E. Soriano and J. Marco-Contelles, *Acc. Chem. Res.*, 2009, **42**, 1026–1036.

45 A. Fürstner and C. Aïssa, *J. Am. Chem. Soc.*, 2006, **128**, 6306–6307.

46 E. Soriano and J. Marco-Contelles, *J. Org. Chem.*, 2007, **72**, 1443–1448.

47 O. N. Faza, C. S. López, R. Álvarez and A. R. De Lera, *J. Am. Chem. Soc.*, 2006, **128**, 2434–2437.

48 C. Nieto-Oberhuber, P. Pérez-Galán, E. Herrero-Gómez, T. Lauterbach, C. Rodríguez, S. López, C. Bour, A. Rosellón, D. J. Cárdenas and A. M. Echavarren, *J. Am. Chem. Soc.*, 2008, **130**, 269–279.

49 Y. Liu, D. Zhang, J. Zhou and C. Liu, *J. Phys. Chem., A.*, 2010, **114**, 6164–6170.

50 C. Landis and F. Weinhold, *J. Comput. Chem.*, 2007, **28**, 198–203.

51 D. Benitez, N. D. Shapiro, E. Tkatchouk, Y. Wang, W. A. Goddard and F. D. Toste, *Nat. Chem.*, 2009, **1**, 482–486.

This journal is © The Royal Society of Chemistry 2013

Org. Biomol. Chem., 2013, **11**, 336–343 | **343**